Harmonic generation in preionized liquid plasmas driven by intense midinfrared pulses

Tomoya Mizuno,* Tianqi Yang, Takayuki Kurihara,† Yimin Gu, Tomoyuki Shoji, Teruto Kanai, and Jiro Itatani‡
The Institute for Solid State Physics, The University of Tokyo, 5-1-5 Kashiwanoha, Kashiwa, Chiba 277-8581, Japan

(Received 28 May 2025; accepted 9 October 2025; published 31 October 2025)

We investigated harmonic generation in preionized liquid ethanol and water driven by linearly polarized midinfrared (MIR) pulses at a center wavelength of 3100 nm. The liquid targets were preionized by a near-infrared pump pulse at 800 nm, enabling systematic control of the electron density in the liquids. At low pump intensities, the harmonic spectra remain unchanged. In contrast, at intermediate pump intensities, the spectra exhibit pronounced target- and delay-dependent modifications, reflecting changes in the optical properties of the ionized liquids. At high intensities, where the electron density exceeds the critical plasma density for MIR light, harmonic yields are strongly suppressed and spectral broadening disappears. Numerical simulations based on the nonlinear propagation model, incorporating plasma and Kerr effects, qualitatively reproduce the experimental observations above the critical plasma density and confirm the significant role of plasma shuttering in harmonic generation. The observation of narrow harmonic spectra provides clear evidence of evanescent-field-induced harmonic generation in preionized liquids. This highlights the potential of ionized liquid plasmas as a robust platform for exploring strong-field phenomena driven by intense and spatially nonuniform fields, beyond the damage thresholds of conventional materials.

DOI: 10.1103/1mtc-m2gt

I. INTRODUCTION

High-order harmonic generation (HHG) in gases has been a cornerstone of attosecond science [1,2]. Precise control of phase-matching conditions, optimizing the gas pressure, Gouy phase, and electron density, has enabled the generation of attosecond pulses in the extreme ultraviolet (EUV) to soft x-ray regions, significantly advancing attosecond science. Recently, HHG in solids has also emerged in attosecond science [3–6]. It was revealed that the spectral and angular behavior of solid HHG is influenced by nonlinear propagation in the solids and is important for understanding the generation mechanism [7–9]. However, it is still challenging to use solid targets in destructive experiments, which limit the usable range of laser intensities to 10^{11}–10^{12} W/cm^2.

In contrast, the use of liquid jets has enabled destructive experiments at higher laser intensities, where tunnel ionization occurs at intensities in the range 10^{13}–10^{14} W/cm^2. In liquids, HHG can extend into the EUV region, making this an important topic of study [10–14]. However, research on nonlinear propagation is still limited. Some studies have focused on harmonic generation in the visible region using intense mid-infrared (MIR) pulses [15,16] to study the effects of nonlinear propagation, but the underlying mechanisms remain unclear. On the other hand, ionized liquid thin-film jets in a strong laser field have been used to generate high-density plasmas, opening new opportunities for research. With the pump–probe setup, an intense prepulse can control the electron density of plasmas through tunnel ionization. This characteristic enables the generation of high-density plasmas with short scale lengths. As a result, applications such as plasma shutter and relativistic HHG have been demonstrated at a repetition rate of 1 kHz [13,14]. HHG on a plasma mirror, where the electron density exceeds the critical plasma density, is considered a promising technique for generating intense attosecond pulses in the EUV ranges.

On the theoretical side, simulations of laser-induced plasma in liquid water have been performed using nonadiabatic *ab initio* molecular dynamics (MD), assuming sub-10-fs pulses at 800 nm [17]. These simulations show that plasmas in liquid water can be categorized into three regimes depending on the laser intensity. At low intensities ($I < 5.3 \times 10^{13}$ W/cm^2), ionization and fragmentation of water molecules are negligible, as water is transparent to near-infrared (NIR) pulses at a wavelength of 800 nm. Conversely, at high intensities ($I > 7.6 \times 10^{13}$ W/cm^2), significant numbers of electrons and protons are generated, leading to the formation of radicals and fragments in the liquid water plasma. More than 50% of solvent molecules dissociate, resulting in drastically reducing the number of intact molecules available for solvation. As a result, the electron relaxation time in such highly ionized and fragmented liquid water is also predicted to be significantly longer than in pure liquid water, due to the drastic reduction in the number of intact solvent molecules. In other words, a free electron in the liquid plasma is expected to survive a long time without electron solvation, because most solvent molecules are ionized and

*Contact author: mizuno.tomoya@issp.u-tokyo.ac.jp
†Present address: Department of Basic Sciences, Graduate School of Arts and Sciences, The University of Tokyo, 3-8-1 Komaba, Meguro-ku, Tokyo 153-8902, Japan.
‡Contact author: jitatani@issp.u-tokyo.ac.jp

Published by the American Physical Society under the terms of the Creative Commons Attribution 4.0 International license. Further distribution of this work must maintain attribution to the author(s) and the published article's title, journal citation, and DOI.

fragmented. Furthermore, these simulations also predict the formation of a metallic state of the liquid water plasma due to a large number of free electrons under these conditions. At intermediate intensities ($5.3 \times 10^{13} < I < 7.6 \times 10^{13}\,\mathrm{W/cm^2}$), tunneling ionization begins, followed by some fragmentation, but the electron density remains below the critical plasma density. Consequently, the resulting state is not metallic in this intensity range, although it differs from pure liquid water.

Based on the Drude model, which assumes that electrons in the media are free, when the electron density exceeds the critical plasma density, the refractive index becomes purely imaginary, resulting in total reflection and the formation of an evanescent field near the surface. These behaviors are characteristic of a metallic optical response. Below the critical plasma density, the refractive index decreases as the electron density increases. In ionized liquids, changes in the refractive index are thus important for understanding the effects of nonlinear propagation on harmonic generation. Although the Drude model has been applied to liquids [18,19], it might be too simplistic to quantitatively describe changes in the refractive index, especially in polar liquids where free electrons are rapidly solvated [20,21]. Very recently, the terahertz response of liquids has been tuned by creating a solvated electron [22]. This approach relies on the fact that the dielectric function of polar liquids is well described by the local-field model of Clausius and Mossotti, which treats electrons and solvent molecules as interacting pointlike dipoles. On the other hand, as mentioned above, in highly ionized and fragmented liquid plasmas the number of intact solvent molecules is greatly reduced, allowing free electrons to survive for a long time. In such a regime, the Drude model—assuming the presence of free electrons—can serve as a reasonable approximation. Indeed, at laser intensities of $10^{13\text{-}14}\,\mathrm{W/cm^2}$, the reflectivity behavior of laser-induced liquid plasmas of water and ethanol can be well understood by a quasifree-electron model, considering band filling and free-electron response to the laser field [19]. Actually, the model is approximated by the Drude model, only considering free-electron response.

In this work we have investigated harmonic generation in preionized liquid ethanol and water driven by MIR pulses, with controlled preionization induced by NIR-pump pulses. The NIR-pump pulse causes tunneling ionization, thereby generating free electrons in the liquid. We can control the electron density produced in the liquid by varying the NIR-pump intensity. This enables the preparation of free electrons in the liquid above and below the critical plasma density. We have used this approach to explore the intense MIR-driven harmonics in preionized liquids at various electron densities, recording the harmonic spectra in the visible spectral range as a function of the time delay between the NIR-pump and MIR-drive pulses.

We first observed the spectral broadening of the harmonic spectra driven only by the intense MIR pulse, without the NIR pump. This broadening is attributed to the plasma-shutter effect induced by the MIR pulse itself. When the electron density in the ionized liquid water exceeds the critical plasma density, the ionized liquid becomes a plasma mirror. The MIR-drive pulse cannot propagate through such a preionized liquid, and an evanescent field is formed near the liquid's surface, causing spectral changes.

At high NIR-pump intensities in the pump–probe experiments, the broadening of the harmonic spectra disappears and the harmonic yields decrease, independent of the targets. Above the critical plasma density, the real part of the refractive index becomes zero. In other words, the refractive index becomes purely imaginary. The exponentially decaying evanescent field appears only in the surface region, indicating that nonlinear propagation effects are suppressed. As a result, this reduces the interaction length, suppressing the harmonic yields. Moreover, the spectral broadening is also suppressed. These observations can be explained qualitatively by solving the nonlinear propagation equation in the liquid. We have confirmed that these behaviors are attributed to the evanescent-field-induced harmonic generation and thus that the plasma-shutter effect plays a significant role in harmonic generation in liquids in transmission geometry in the high-intensity region ($I > 10^{14}\,\mathrm{W/cm^2}$). Our results clearly demonstrate that highly ionized and fragmented liquid plasmas provide a robust platform for studying strong-field phenomena driven by intense and spatially nonuniform evanescent fields, beyond the damage thresholds of conventional materials.

At intermediate NIR-pump intensities, we observed target- and time-delay-dependent harmonic spectra. In this region, the NIR-pump pulse induces tunneling ionization, but the electron density remains below the critical plasma density. The ionized liquid targets are therefore not metallic, but they differ from the pure liquids. The time-dependent harmonic spectra cannot be reproduced accurately by the Drude model, which considers only free-electron plasma. These results indicate that a more-sophisticated model—which accounts for fragments and radicals in the ionized liquids—is necessary to describe the optical properties in ionized liquids adequately below the critical plasma density.

The paper is organized as follows. In Sec. II we outline the experimental setup and procedure. In Sec. III we present the nonlinear propagation simulation and scaling of the harmonics. In Sec. IV we discuss the experimental and theoretical results. Section V concludes the paper.

II. EXPERIMENTS

We used a $KTiOAsO_4$ (KTA)-based optical parametric amplifier pumped by a Ti:sapphire chirped-pulse amplification system to generate intense femtosecond MIR optical pulses at a center wavelength of 3100 nm and a pulse duration of 160 fs without multiplate compression [23,24]. We focused the linearly polarized MIR pulses into a flat liquid jet using a CaF_2 lens with a focal length of 50 mm. The NIR-pump pulse, at a center wavelength of 800 nm with a pulse duration of 50 fs, was provided by the same Ti:sapphire pump laser and was also focused into the jet by a CaF_2 lens with a focal length of 100 mm. We measured the $1/e^2$ diameters of the MIR-drive and NIR-pump pulses at the focus to be 21 and 46 μm, respectively. The intensities of the MIR and NIR pulses were estimated from the measured pulse energies, beam diameters at focus ($1/e^2$) with an approximate error of 10%, and pulse durations. The overall uncertainty is estimated to be around ±20%, primarily due to variations in the beam

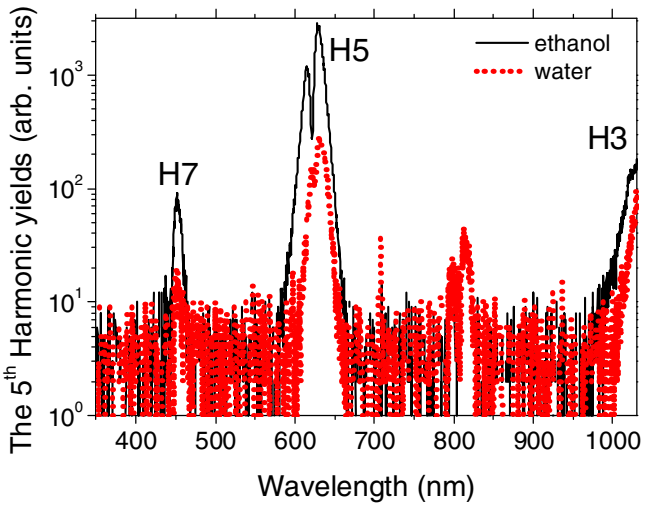


FIG. 1. The harmonic spectra obtained from liquid ethanol and water driven by the MIR pulse at the intensity of $1 \times 10^{14}\,\mathrm{W/cm^2}$. The peak near 800 nm arises from residual stray NIR-pump light.

profile measurements, while other sources of error are considered negligible.

To produce the flat liquid jet targets, we employed a monolithic metallic nozzle with a compressed-tube orifice (FEMTO Deployments, Inc.) [25] and a stable diaphragm pump (TACMINA Corp., Smooth-Flow Q series) operating at a flow rate of 60 mL/min. We measured the thickness of the jet to be between 4 and 8 μm. Liquid ethanol and water were used as the target media. Harmonic spectra were recorded in transmission geometry using a fiber-coupled, thermoelectric-cooled spectrometer (Ocean Optics, USB2000).

We generated harmonics by the MIR pulses in the flat liquid jets of either ethanol or water. Figure 1 shows the harmonic spectra generated in liquid ethanol and water only by the MIR pulse, without the NIR-pump pulses. The fifth (H5) and seventh (H7) harmonics are clearly visible, as is the tail of the third (H3) harmonic. The harmonic yield of ethanol is approximately one order of magnitude higher than that of water, consistent with reported results using 1600-nm few-cycle pulses [10].

To study the role of electron plasma effects on nonlinear propagation and harmonic generation in preionized liquids, we conducted experiments using an NIR pump and an MIR probe, with both pulses polarized parallel to each other. Although ethanol and water are transparent to 800-nm light in linear optical processes, the intense NIR pump can induce tunneling ionization. After preionization by the NIR pump, the MIR pulse generates harmonics in the preionized liquid plasma. We recorded the harmonic spectra as a function of the time delay between the NIR-pump and the MIR-drive pulses. In this work, nth-order harmonics are denoted as Hn.

III. SIMULATION OF NONLINEAR PROPAGATION AND HARMONIC GENERATION IN A LIQUID

In this section we numerically simulate the nonlinear propagation and harmonic generation in liquid media. We model the linearly polarized beam described by the envelope $\mathcal{E}(z,t)$ of the electric field $\mathbf{E}$, expressed as $\mathbf{E} = \mathrm{Re}[\mathcal{E}(z,t)\exp(ikz - i\omega_0 t)]$, where z denotes the coordinate along the propagation axis, and the origin ($z = 0$) is defined at the liquid surface. Here, λ_0, $k_0 = \omega_0/c = 2\pi/\lambda_0$, $k = n_0 k_0$, and ω_0 denote the wavelength in vacuum, the wave number in vacuum, the wave number in liquid media—with the real part of the linear refractive index n_0—and the carrier frequency, respectively. The speed of light is denoted by c. In our experiments, n_0 is 1.38 for liquid ethanol and 1.48 for water at a wavelength of 3100 nm, respectively [26,27]. The input beam is assumed to be Gaussian, with a peak electric field $\mathcal{E}_0$ and pulse duration T (FWHM in intensity), given by

$$\mathcal{E}(z=0,t) = \mathcal{E}_0 \exp[-2\ln 2(t/T)^2]. \tag{1}$$

We assume that $\mathcal{E}(z,t)$ varies slowly with respect to both z and t, allowing it to be described by the propagation equation [28,29] in the reference frame moving at the group velocity v_g, written below,

$$\frac{\partial \mathcal{E}}{\partial z} = ik_0[n(z,\tau) - n_0]\mathcal{E} - \frac{1}{2}\frac{W(|E|)U_i}{|\mathcal{E}|^2}(\rho_n - \rho_e)\mathcal{E} - k_0\kappa\mathcal{E}, \tag{2}$$

where $\tau = t - z/v_g$ is the retarded-time variable, $n(z,\tau)$ is the instantaneous refractive index, ρ_n and ρ_e are the density of neutral molecules and of electrons in the liquid, and κ is the imaginary part of the linear refractive index. At 3100 nm, κ is 0.6 for liquid ethanol and 0.18 for water [26,27], reflecting resonant absorption of OH vibrational modes. The quantities W and U_i represent the tunneling ionization rate and the ionization potential of a solvent molecule, respectively, with U_i taken as 10.48 eV for ethanol and 12.62 eV for water [30]. In Eq. (2) we have neglected the term $-i\frac{k''}{2}\frac{\partial^2\mathcal{E}}{\partial\tau^2}$, where k'' is the second-order dispersion coefficient—which describes the group velocity dispersion—because it is negligibly small for the thickness of our experimental liquid jet (several micrometers). The refractive index $n(z,\tau)$, based on the Drude model including the Kerr effect [18], is given by

$$n(z,\tau) \approx \sqrt{n_0^2 + 2n_0 n_2 I - \frac{4\pi e^2 \rho(z,\tau)}{m_e \omega_0^2}}, \tag{3}$$

where n_2 is the second-order nonlinear refractive coefficient due to the Kerr effect, I is the field intensity, and m_e and e are the electron mass and charge, respectively. Above the critical density, n becomes a pure imaginary number, leading to total reflection and the formation of an evanescent field, which is the so-called plasma-shutter effect. A decaying evanescent field appears inward from the preionized liquid surface. It might be helpful to provide a physical picture of this process. When the carrier frequency of light falls below the critical plasma frequency of a medium, the oscillating electric field induces free electrons in the medium to move in a manner that opposes the incident field. This collective electron motion generates an internal polarization that effectively shields the medium from the external field, resulting in total reflection—a phenomenon commonly referred to as the plasma-shutter effect. This behavior is well known in plasmas and metallic solids, where it leads to a well-defined critical plasma frequency below which electromagnetic waves cannot propagate. The critical plasma density is given by $n_0^2\rho_c$,

where ρ_c represents the critical plasma density for $n_0 = 1$. This quantity is $\rho_c = 1.16 \times 10^{20}\,\mathrm{cm}^{-3}$ for the MIR wavelength at 3100 nm and is $\rho_c = 1.73 \times 10^{21}\,\mathrm{cm}^{-3}$ for the NIR wavelength at 800 nm. We used $n_2 = 7.7 \times 10^{-16}\,\mathrm{cm}^2/\mathrm{W}$ for liquid ethanol and $4.1 \times 10^{-16}\,\mathrm{cm}^2/\mathrm{W}$ for water. These are the values at 800 nm [31], due to the lack of data at 3100 nm. The Kerr effect is negligible compared to the plasma effect at our experimental intensity. Thus, the uncertainty in this value does not significantly affect our simulation results.

The time evolution of electron density ρ_e satisfies the rate equation [28,29,32], given below:

$$\frac{\partial \rho_e}{\partial \tau} = W(|E|)(\rho_n - \rho_e). \tag{4}$$

The right-hand side of Eq. (4) describes tunneling ionization, and we neglect avalanche ionization. In Ref. [33] it is discussed that the avalanche effect is negligible in liquid ethanol and in water for an ultrafast pulse of 150 fs. In our case the pulse durations are 160 fs for the MIR pulses and 50 fs for the NIR pulses, so the avalanche ionization is negligible for our experiments. We calculated the tunneling ionization rate W using the Ammosov-Delone-Krainov (ADK) theory [34], assuming a hydrogenlike target, although the detailed tunneling mechanism in liquids remains an open question [20,35,36].

Based on the perturbative scaling, the Hn dipole induced by an MIR pulse can be written as

$$P^{(n)}(z,t) = \mathrm{Re}[\chi^{(n)}[\mathcal{E}(z,t)\exp(ikz - i\omega_0 t)]^n], \tag{5}$$

where $P^{(n)}$ represents the nth-order dipole, and $\chi^{(n)}$ represents the nth-order nonlinear susceptibility. We integrate the nth-order dipole $P^{(n)}$ over the coordinate z to obtain the harmonic signal, considering only linear propagation of the generated harmonics. This approach combines the use of ADK tunneling ionization rates with a perturbative scaling for harmonic dipoles. Under our experimental conditions ($\sim 10^{14}\,\mathrm{W/cm}^2$), tunneling dominates rather than multiphoton process, according to the Keldysh theory [37], so the ADK theory is valid for our condition, while the perturbative treatment is used to qualitatively capture spectral modifications. In our study we mainly focus on the fifth harmonic (H5). For H5 at 620 nm, the refractive indices n_0 are approximately 1.35 for ethanol and 1.32 for water [26,27]. While perturbative theory may not be fully accurate at intensities around $10^{14}\,\mathrm{W/cm}^2$, it still provides qualitative insights into spectral modifications due to nonlinear propagation. For simplicity, we set $\chi^{(5)}$ to be constant, noting that this significantly affects absolute yields but not the relative spectral evolution or intensity dependence.

IV. RESULTS AND DISCUSSION

A. The intensity-dependent H5 yields

Figure 2 shows the measured and calculated intensity-dependent H5 yields from liquid ethanol and water driven by the MIR pulse. The results clearly exhibit good agreement between the measured and calculated yields. In both cases we find that the yields become saturated at intensities in the high $10^{13}\,\mathrm{W/cm}^2$ range. This saturation behavior is consistent with previous results, which we obtained using slightly different MIR pulses at a wavelength of 3250 nm and with a pulse duration of 70 fs, employing multiplate compression [24]. We also observed plasma emission in these experiments, with a threshold close to the onset of H5 saturation. The calculated yields also exhibit saturation behavior, although we calculated them using the perturbative scaling. Our calculations indicate that the saturation of the calculated yields is due to the plasma-shutter effect, which clamps the latter part of the driving-laser pulse. These results clearly show that plasma effects play an important role in harmonic generation in liquids at high intensities. It has already been pointed out that the plasma-shutter and ionization-saturation effects reduce the high-harmonic yields from liquid isopropanol in the EUV range [12]. As mentioned in Sec. I, nonadiabatic *ab initio* molecular dynamics simulations have previously predicted that a metallic water plasma is formed by the NIR (800 nm) pulse, with the plasma generation threshold at $7.6 \times 10^{13}\,\mathrm{W/cm}^2$. This value is in good agreement with our calculation of the plasma-shutter threshold—approximately $8 \times 10^{13}\,\mathrm{W/cm}^2$—obtained using the ADK theory combined with the Drude model.

B. Spectral broadening of the H5 spectra

Figures 3 and 4 show the measured and calculated H5 spectra for liquid ethanol and water, respectively, driven by the MIR pulse for various intensities. We found that the H5 spectra broaden as the intensity increases. The spectral broadening begins at intensities in the high $10^{13}\,\mathrm{W/cm}^2$ range, which are close to the thresholds for plasma emission and the plasma-shutter effect. Furthermore, a double-peak structure appears at high intensities.

To understand the role of the plasma effect in the spectral broadening of the harmonics, we consider their nonlinear propagation in ionized liquids. For ethanol, both the calculated and measured H5 spectra exhibit spectral broadening and a double-peak structure. The calculations show a significant blueshift, which is attributed to the plasma-shutter effect. Moreover, the plasma-shutter effect also causes an abrupt amplitude decrease. The broadening is mainly resulting from the plasma-shutter effect; therefore it starts at the plasma-shutter threshold. Furthermore, even before the electron density reaches the critical plasma density, the increasing free-electron population during the pulse leads to a temporal reduction of the refractive index, i.e., $dn/dt < 0$. This dynamic refractive index change induces a time-dependent phase shift $\phi(t) \propto n(t)$, resulting in a modulation of the instantaneous frequency, given by

$$\omega(t) = \omega_0 + \frac{d\phi}{dt} = \omega_0 + k_0 L \frac{dn}{dt}, \tag{6}$$

where L is the propagation distance [18,29,32]. Since $dn/dt < 0$, the instantaneous frequency shifts to higher values, leading to a spectral blueshift. Furthermore, the abrupt temporal truncation and evanescent-field formation occur when the plasma density exceeds the critical value, providing a comprehensive explanation of the observed spectral shifts.

Although there are some differences between the measured and calculated spectra, the calculations qualitatively reproduce the measured spectra. For water, the measured spectra display a strong redshift and a weaker blueshift. In contrast, the calculations predict only a strong blueshift. Our model calculations for nonlinear propagation do not reproduce

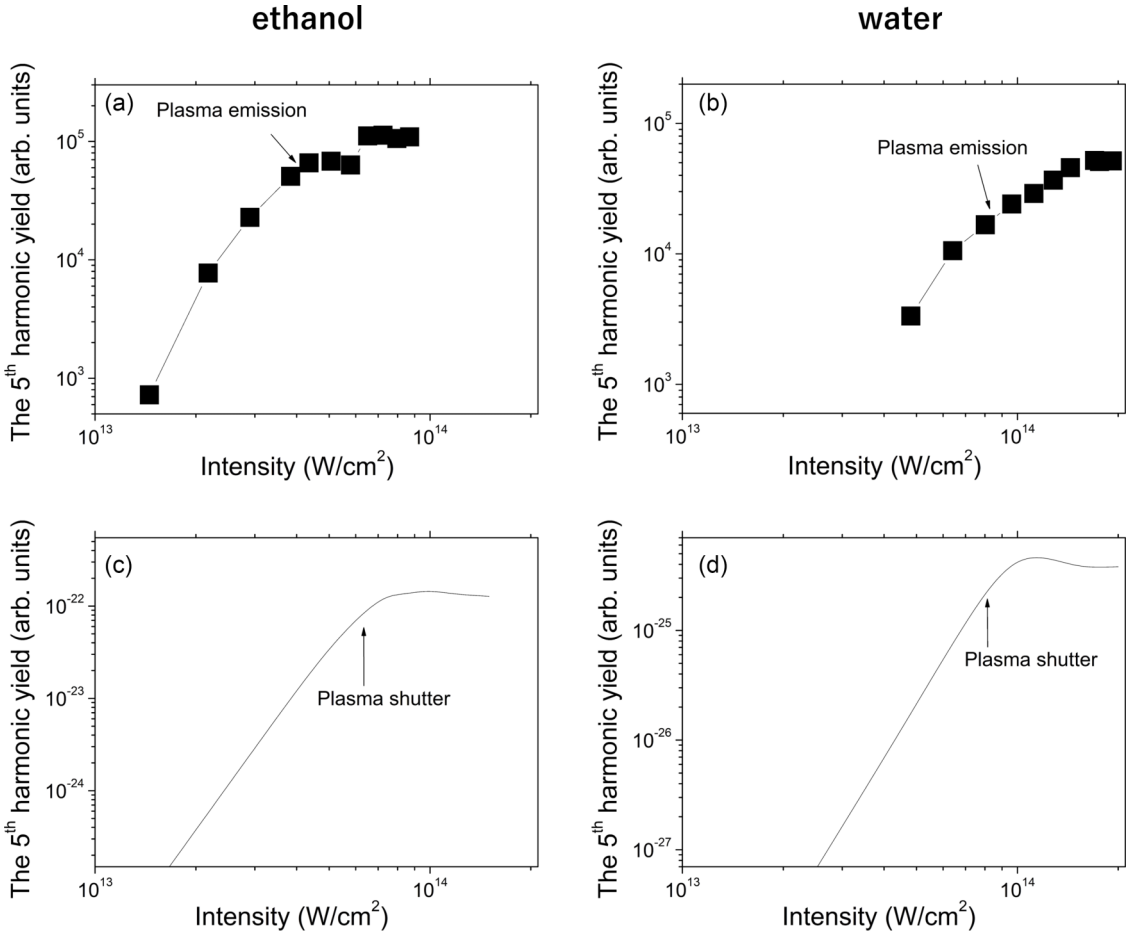


FIG. 2. Measured (a), (b) and calculated (c), (d) intensity-dependent H5 yields from liquid ethanol and water driven by the MIR pulse. In (a), (b) the arrows indicate the obtained threshold for plasma emission, while in (c), (d) they indicate the calculated threshold for the plasma shutter at 3100 nm.

the redshift. The measured spectra for liquid water show a weaker blueshift than for ethanol, which may be attributed to wavelength-dependent absorption of water and ethanol. The peak of the OH-stretching mode in liquid water is located at 2940 nm [27]; consequently, the blue side of the fundamental pulse is more strongly absorbed than the red side. However, we did not consider wavelength-dependent absorption in our calculation. Our model only accounts for the role of the emitted electrons, assuming them to be free electrons. In addition, the ionization of a solvent molecule in a liquid is often accompanied by dissociation and radical formation. To calculate the nonlinear propagation in ionized liquids and reproduce the spectral broadening of harmonics in liquids driven by a high-intensity pulse, we therefore need a more sophisticated approach that accounts for ionization and fragmentation dynamics. We conclude that the plasma-shutter effect plays an important role in nonlinear propagation and harmonic generation above the critical plasma density $n_0^2\rho_c$ in liquid targets, leading to the spectral broadening.

C. Harmonic generation in preionized liquid ethanol and water plasmas

We performed a NIR-pump and MIR-driven harmonic generation experiments to investigate plasma effects on harmonic generation around the critical plasma density $n_0^2\rho_c$ for MIR-drive pulses with a central wavelength of 3100 nm. As mentioned in Sec. II, we use NIR-pump pulses to ionize and excite the liquid targets. By varying the intensity I_{NIR} of the NIR-pump pulses, we can control the electron density ρ_e of the preionized liquid. The intensity I_{MIR} of the MIR-drive pulses is fixed at $8 \times 10^{13}\,\mathrm{W/cm^2}$ for liquid ethanol and $2 \times 10^{14}\,\mathrm{W/cm^2}$ for water, respectively. These MIR intensities allow us to generate electron densities ρ_e that exceed the critical plasma density $n_0^2\rho_c$, leading to the spectral broadening of the harmonics, as shown in Figs. 3 and 4.

Here, we classify three distinct regions of pump intensities: those that generate electron densities that are (1) much lower than, (2) just below, and (3) above the critical plasma density. These regions have already been shown in nonadiabatic *ab initio* MD simulations [17].

1. Time-dependent H5 at high pump intensities

Figure 5 shows the time-dependent H5 harmonics generated by the MIR pulses from preionized liquid ethanol and water as a function of the time delay between the NIR-pump and MIR-drive pulses at high pump intensities. It clearly shows that the harmonic yields decrease after the NIR-pump pulse. The spectral widths remain narrower after

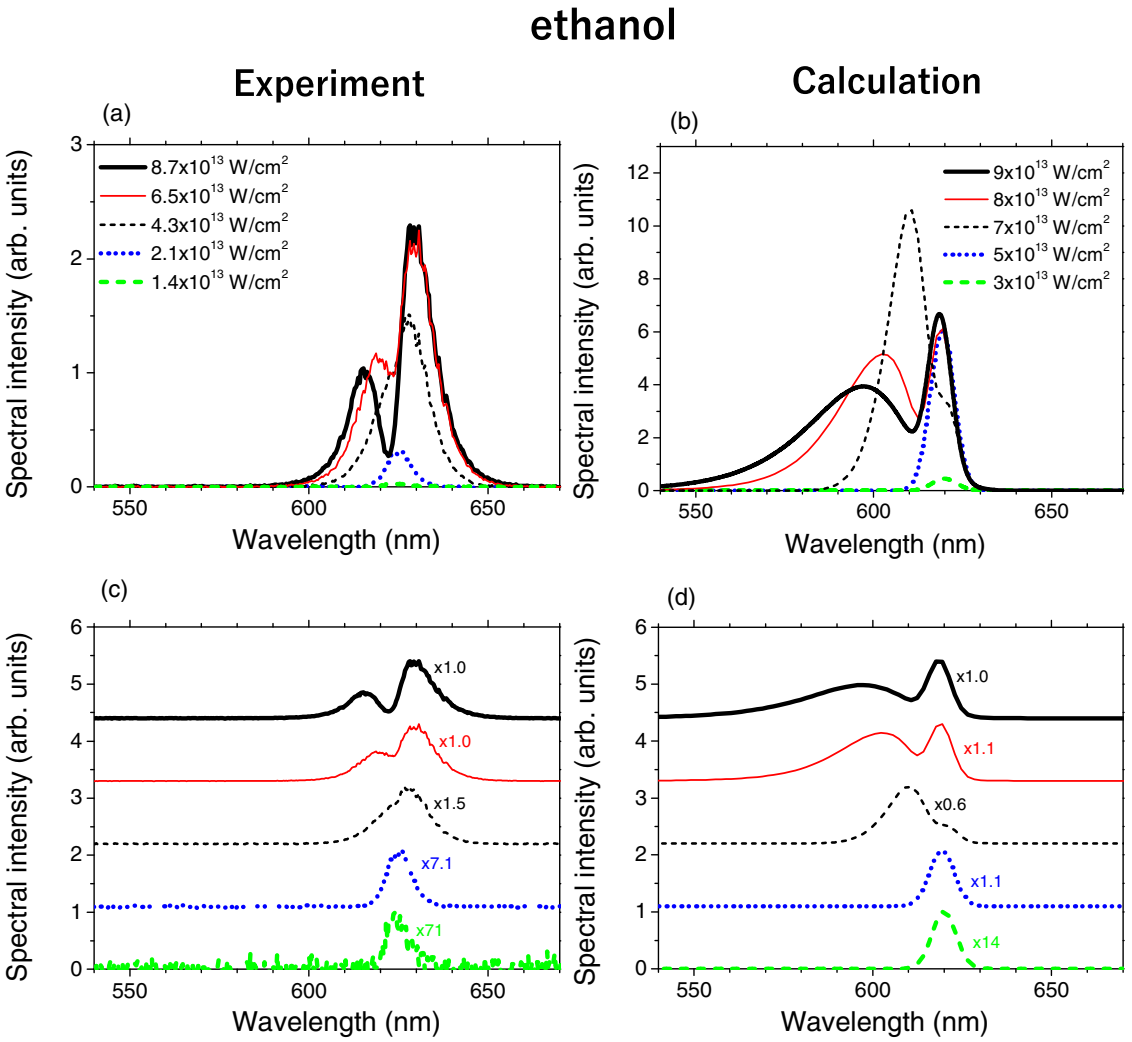


FIG. 3. Experimental and calculated H5 spectra for liquid ethanol for various intensities driven by the MIR pulse. The bottom figures are normalized versions of the upper figures.

the pump, independent of the targets, while spectral broadening of the harmonics occurs before the NIR pump. These delay-dependent harmonic features appear immediately after the pump pulse. In this experiment the NIR-pump intensities were sufficiently high to generate a significant number of electrons in the liquids, resulting in an electron density that exceeded the critical plasma density for the MIR pulse. Under such conditions, the incoming MIR pulse is totally reflected and becomes a decaying evanescent field inside the interface; this is the so-called "plasma-shutter" effect. The solvation dynamics of electrons in liquids are highly solvent dependent: in water, free electrons are solvated in about 300 fs [20], whereas in ethanol, solvation times are several picoseconds [21]. If solvation significantly influenced harmonic generation, the delay-dependent response should differ markedly between water and ethanol. Our results imply that at high pump intensities, free electrons can survive for a long time in ionized and fragmented liquid plasmas without solvation and contribute to the modification of harmonic generation. Moreover, due to the prolonged lifetime of free electrons in highly ionized and fragmented liquid plasmas, the Drude model is considered a valid approximation.

To gain a deeper understanding of the influence of the plasma-shutter effect on harmonic generation in the liquid, we also calculated the harmonic spectra generated from preionized liquids by the NIR pump. In our calculations, the NIR pump only causes ionization, while fragmentation and electron solvation are neglected. Furthermore, we assume that the fifth-order susceptibility $\chi^{(5)}$ does not change between the pure and preionized liquids. Even if this assumption is incorrect, it has little influence on the spectral changes, although it may lead to inaccuracies in the harmonic yields. Thus, we focus mostly on the spectral changes caused by the NIR pump, rather than on changes in the harmonic yield.

Figure 6 shows both the measured and calculated H5 spectra for positive delays (5–15 ps) and for negative delays (<-3 ps). The top figures show the measured integrated spectra for liquid ethanol and for water, respectively. The bottom figures show the spectra calculated with and without the NIR pump. These calculations demonstrate that the H5 spectra become narrow in preionized liquids, irrespective of the targets. These narrow spectra reflect the spectra of the driving MIR pulses. By solving the nonlinear propagation equation, we show that the MIR field in preionized liquid water–in which

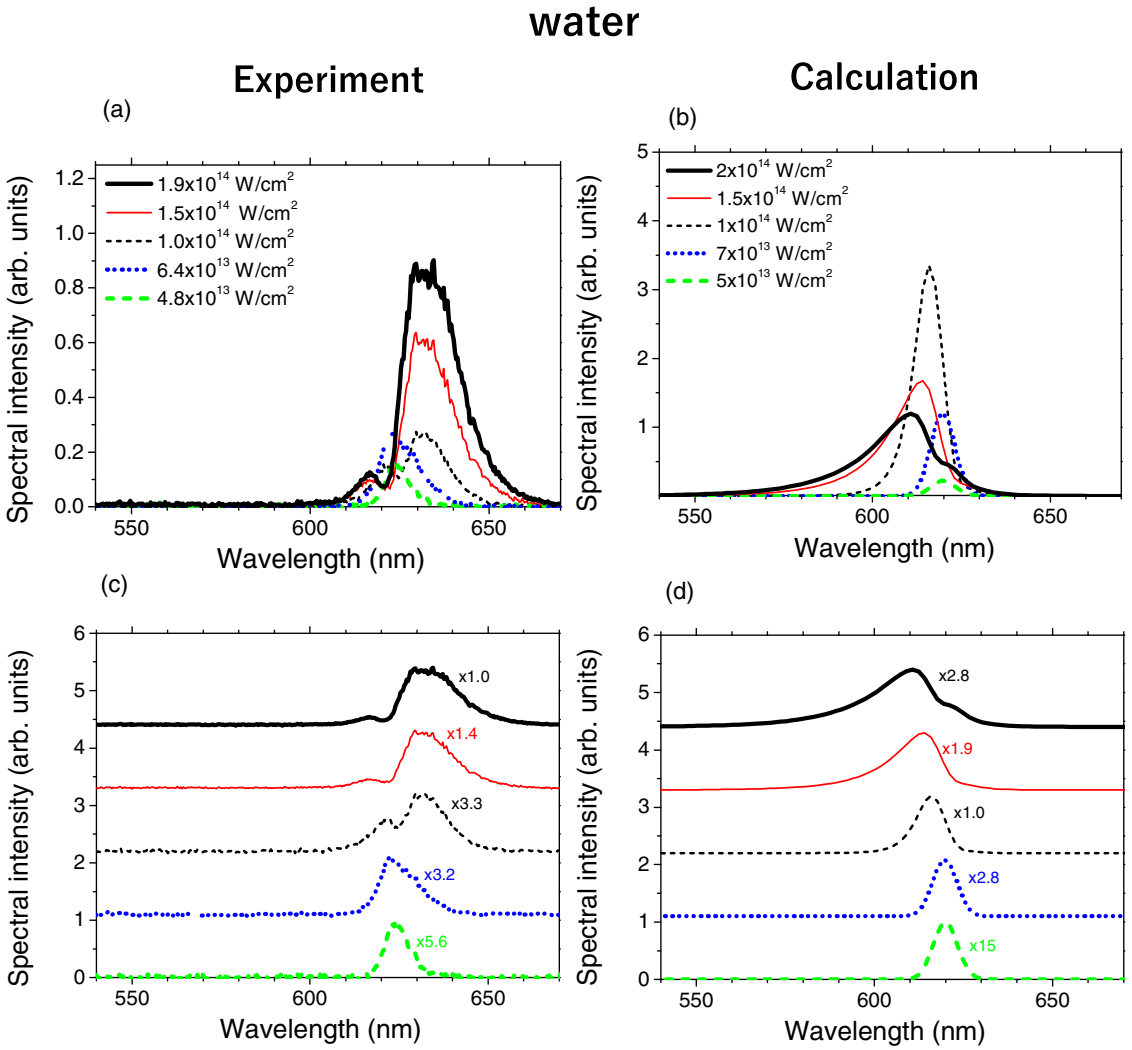


FIG. 4. The same as Fig. 3, but for liquid water.

the electron density exceeds the critical plasma density—decays rapidly due to the plasma-shutter effect (as detailed in Appendix A). Under such conditions, the evanescent field is confined to the vicinity of the interface, which results in an extremely short interaction length and a reduction in the harmonic yields. Furthermore, the spectral broadening of the fundamental MIR pulses is suppressed because the real part of the refractive index becomes zero, causing the phase of the MIR-drive pulse to remain constant. These simulation results are consistent with the observed harmonic behavior. The spectral narrowing and decrease in yield thus provide clear evidence of evanescent-field-induced harmonic generation in liquid plasmas. These phenomena are universal, occurring independently of the targets, when the electron density exceeds the critical plasma density, i.e., when the electronic state of the liquid medium transforms into a metallic state.

In contrast, the change in the H5 yields is not reproduced by our model because of the assumption that the value of $\chi^{(5)}$ remains constant between the pure and preionized liquids. The suppression of the harmonic yield is much more pronounced in the calculations (∼160) than in the experiments (∼6.2) for ethanol, whereas better agreement is observed for water. This is likely due to our assumption of a constant $\chi^{(5)}$, which ignores possible modifications due to molecular fragmentation, while the effect of electron solvation becomes minor. Moreover, we speculate that ionization is accompanied by fragmentation and radical formation in the liquids, leading to changes in their optical properties. A more detailed treatment incorporating such effects is beyond the scope of this work but will be an important subject for future studies. Given the lack of a simplified model that can account for these processes, first-principles simulations are necessary to accurately describe such phenomena in harmonic generation in liquid plasmas [38].

2. Time-dependent H5 at intermediate pump intensities

Figure 7 shows the time-dependent H5 spectra of liquid ethanol and water at the pump intensities $6 \times 10^{13}\,\mathrm{W/cm^2}$ and $9 \times 10^{13}\,\mathrm{W/cm^2}$. Although these pump intensities are sufficient to generate a substantial number of free electrons in the liquids, the electron densities remain just below the critical plasma density for the MIR pulses at 3100-nm wavelength. The results display a pronounced dependence on both

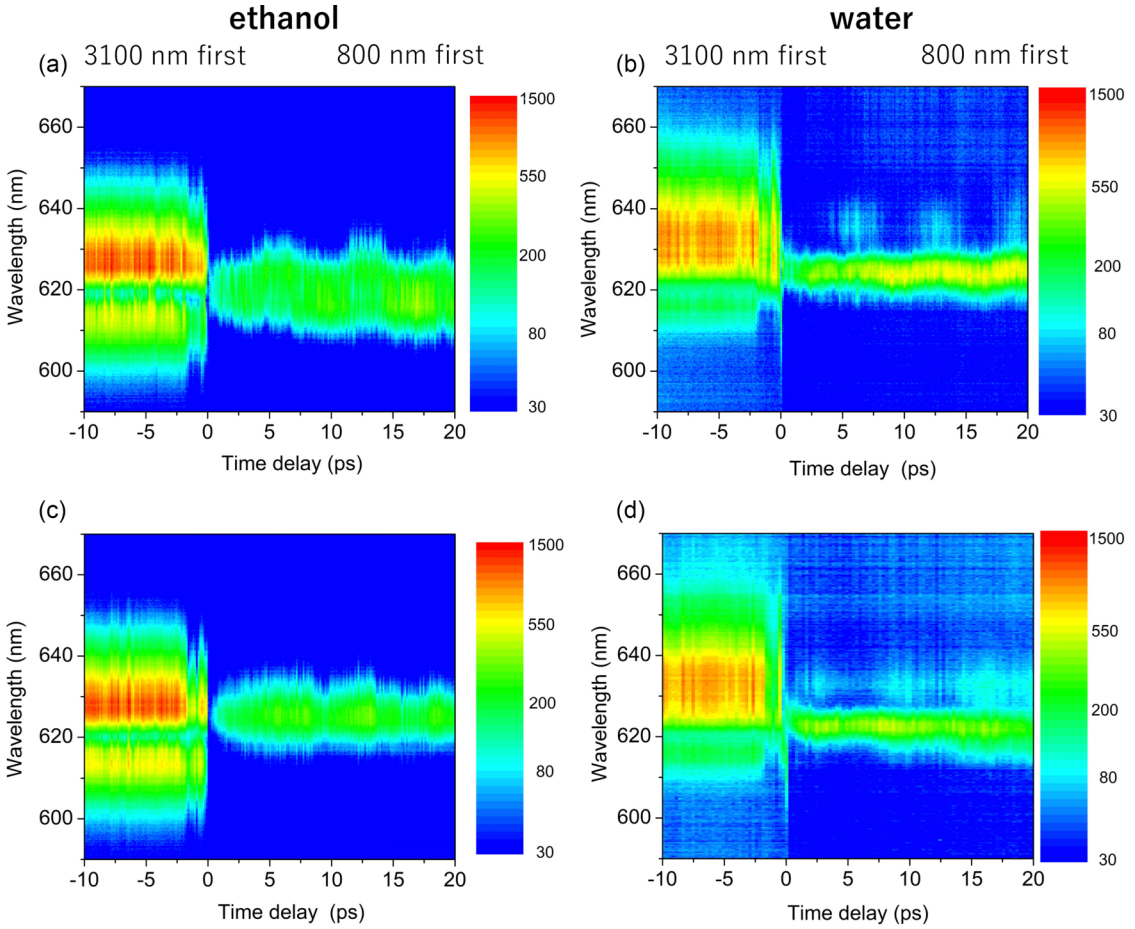


FIG. 5. H5 spectra for liquid ethanol and water as a function of the delay time. The top figures (a), (b) are for liquid ethanol and water at the NIR-pump intensities of 9×10^{13} W/cm^2 and 1.3×10^{14} W/cm^2, respectively. The bottom figures (c), (d) are the same as the top figures, but for the NIR-pump intensities of 1.3×10^{14} W/cm^2 and 2×10^{14} W/cm^2, respectively.

the targets and the pump–probe delay time. For ethanol, the position of the H5 spectral peak shifts after the pump, accompanied by a decrease in the harmonic yields. In contrast, for water we observed a similar spectral shift; however, the H5 yield slightly increases after the pump, probably due to the change of the phase-matching condition and interaction length [24].

Figure 8 compares the measured H5 spectra with those calculated for both liquid ethanol and water at positive (5−15 ps) and negative delays (<-3 ps). These intermediate intensities of the NIR-pump pulse can induce significant changes in the optical properties of the liquids below the critical plasma density. These results indicate that simulations that incorporate only the free-electron plasma effect based on the Drude model fail to reproduce the experimental spectra accurately. This suggests that the contribution of the free electrons alone is insufficient to fully describe the optical response of an ionized liquid below the critical plasma density. In this case, as mentioned before, an electron is rapidly solvated. As a result, the Drude model is not a good approximation, because the electron is not free in polar liquid. Therefore, a more comprehensive model—one that incorporates the effects of the molecular fragments and radicals generated in the ionized liquid and solvation process—is necessary to achieve better agreement with the experimental results.

3. Time-dependent H5 at low pump intensities

Figure 9 shows the time-dependent H5 spectra of liquid ethanol and water at a pump intensity of 4.5×10^{13} W/cm^2. At this lower intensity, the spectra exhibit negligible delay-time dependence, except in the region where temporal overlap between the pump and probe pulses occurs. Such a low pump intensity is insufficient to induce nonlinear optical processes, resulting in almost no tunneling ionization and fragmentation. Furthermore, both ethanol and water are essentially transparent to the NIR-pump pulse at 800 nm. The electron densities generated in liquid ethanol and water by the NIR pump at the surface ($z = 0$) are estimated to be 4.3×10^{18} cm^{-3} and 5×10^{17} cm^{-3}, respectively. Thus, the pump pulse causes very small change in the optical properties of liquid ethanol or water. According to calculations based on the Drude model, the corresponding change in the refractive index n is only $\sim 10^{-3}$. This minor variation indicates that the NIR-pump pulse induces virtually no change in the optical properties of the liquid under these conditions.

V. CONCLUSIONS

We have investigated harmonic generation in preionized liquid ethanol and water driven by intense MIR pulses, with

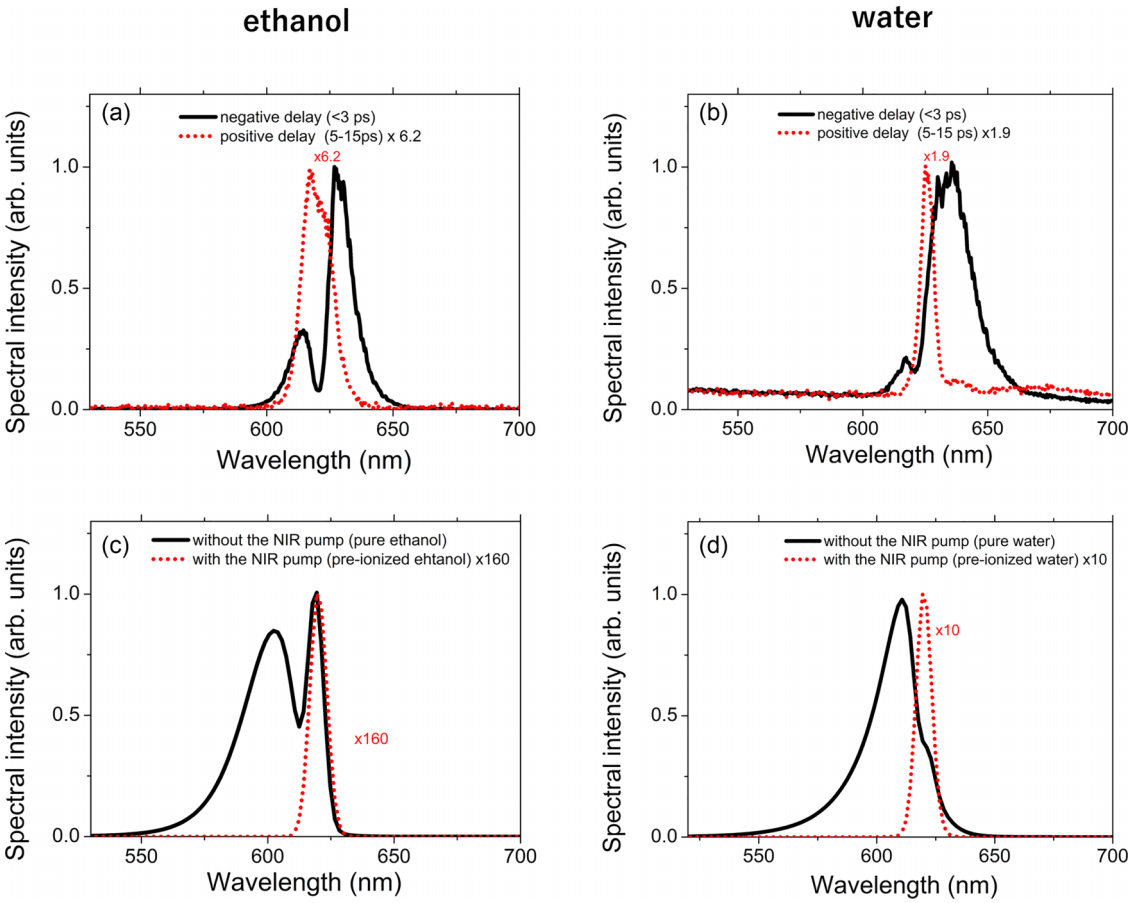


FIG. 6. Measured (a), (b) and calculated (c), (d) integrated H5 spectra for liquid ethanol (a), (c) and water (b), (d) at the NIR-pump intensities of 9×10^{13} W/cm^2 and 1.3×10^{14} W/cm^2, respectively. The spectra are normalized to unity at the maximum. Spectra at positive delays are shown scaled by the indicated factors relative to the spectra at negative delays.

controlled electron densities achieved via an NIR pump. We observed both spectral broadening and harmonic yield saturation, and our numerical simulations based on nonlinear propagation equations show that these phenomena arise from nonlinear propagation and the plasma-shutter effect. These results highlight the crucial role of plasma effects in the nonlinear optical response of liquids at high intensities. To further elucidate the role of the plasma effect on harmonic generation in liquids, we performed a NIR-pump and MIR-drive experiment. When the electron density exceeded the critical plasma density for MIR light, we observed a suppression of spectral broadening and a significant reduction in

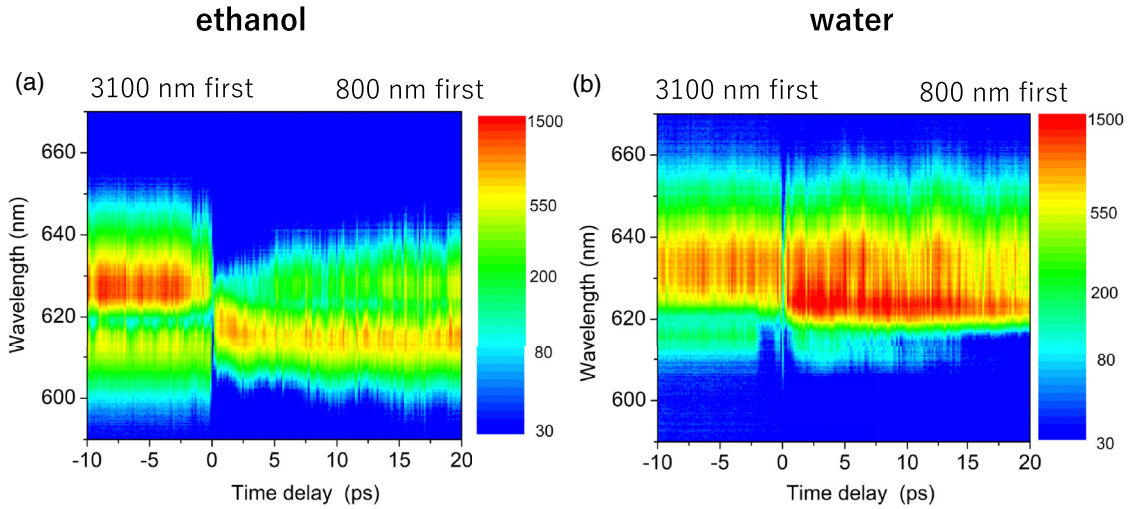


FIG. 7. The same as Fig. 5, but at the NIR-pump intensities (a) 6×10^{13} W/cm^2 for liquid ethanol and (b) 9×10^{13} W/cm^2 for water.

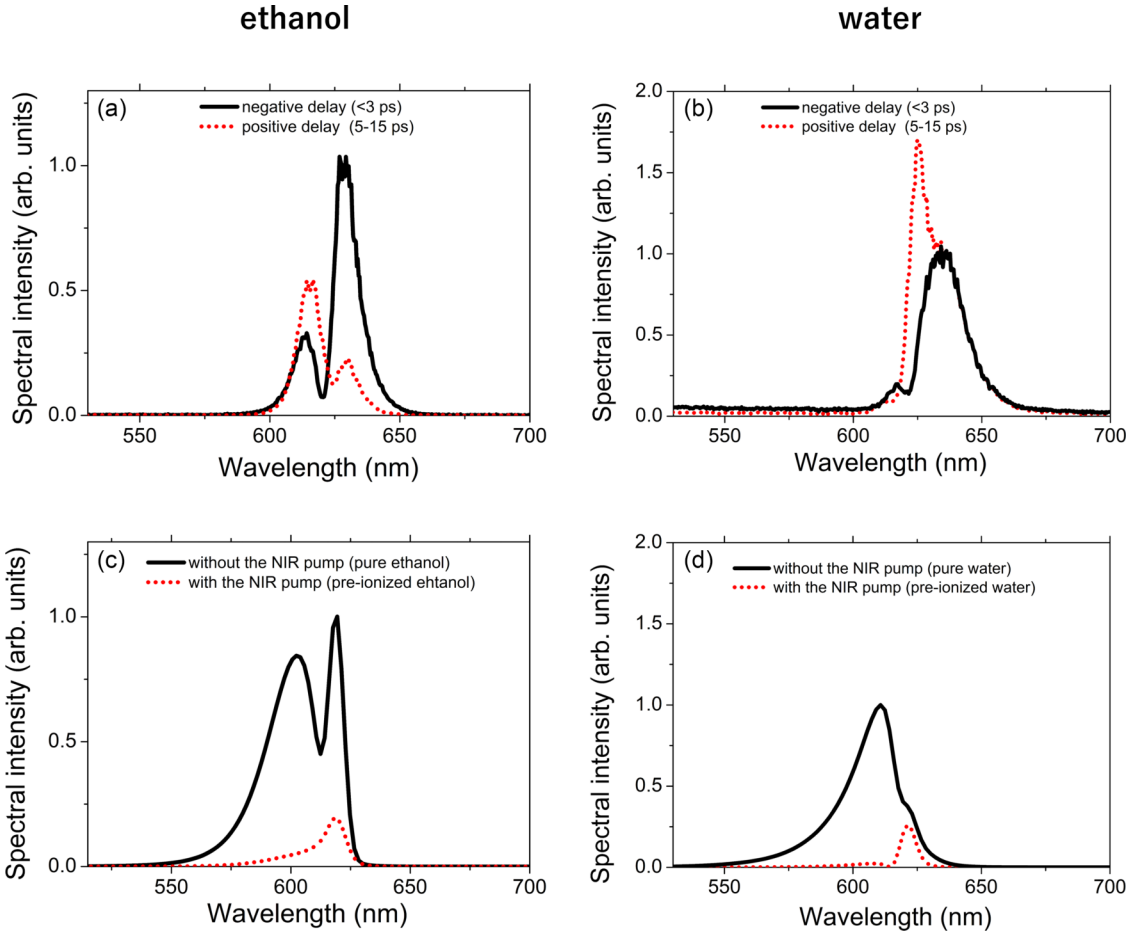


FIG. 8. Measured (a), (b) and calculated (c), (d) integrated H5 spectra from liquid ethanol (a), (c) and water (b), (d) at the NIR-pump intensities of 6×10^{13} W/cm^2 and 9×10^{13} W/cm^2, respectively. The spectra for negative delays are normalized to unity at the maximum. Spectra at positive delays are also normalized by the same factors as the spectra at negative delays.

harmonic yields, regardless of the target liquid. These features appear immediately after the pump pulse and are attributed to the plasma-shutter effect induced by the NIR-pump pulse, as qualitatively reproduced by our theoretical model. Under such conditions, the MIR pulse becomes an evanescent field in the preionized liquid plasma, leading to rapid spatial decay of the incident waves. These observations provide clear experimental evidence of evanescent-field-induced harmonic generation in preionized liquid plasmas. We have experimentally confirmed that, regardless of the target liquid, the

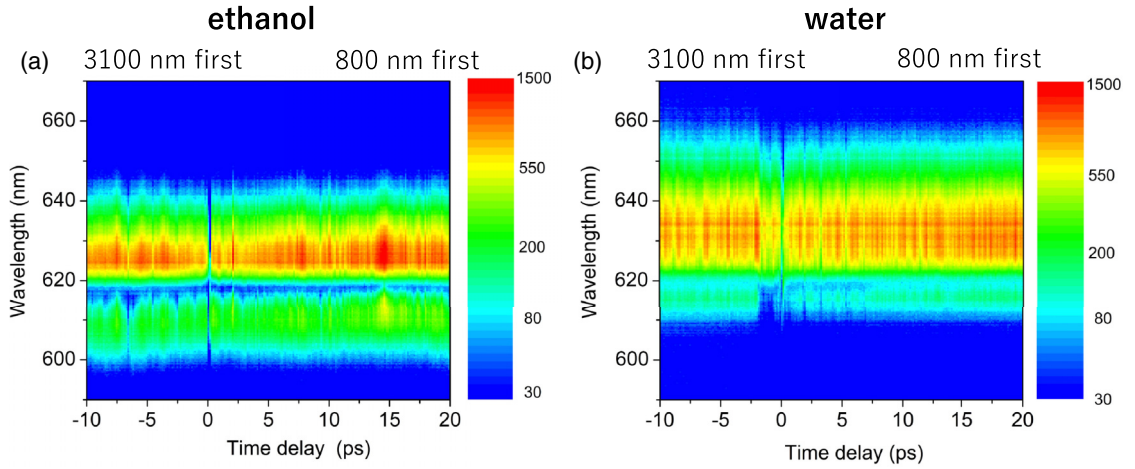


FIG. 9. (a) H5 spectra for liquid ethanol as a function of delay time. (b) The same as (a) but for liquid water. The pump intensity is 4.5×10^{13} W/cm^2.

electronic response of the liquid plasma becomes metallic under these conditions. In such a case, the Drude model is a good approximation, because an electron in such a liquid plasma can survive for a long time.

Furthermore, we found that when the electron density is just below the critical plasma density, the harmonic spectra exhibited a strong dependence on both the pump–probe delay and the target medium. These features suggest that the optical properties of ionized liquids cannot be fully described by the free-electron Drude model alone. Effects involving molecular fragments and radicals, and electron solvation likely play a significant role. At lower pump intensities, where tunneling ionization is negligible, the harmonic spectra remained essentially unchanged, confirming that the observed modifications are indeed plasma-induced.

In conclusion, the plasma-shutter effect plays a dominant role in harmonic generation from highly ionized liquids under high-intensity irradiation ($I > 10^{14}\,\mathrm{W/cm^2}$) in transmission geometry. Under these conditions, the MIR pulse becomes an intense and spatial nonuniform evanescent field within the liquid plasma. Our results demonstrate that highly ionized liquid plasmas can serve as a unique and damage-resistant medium for generating evanescent fields under strong-field conditions. Unlike metamaterials or solid-state nanostructures [39–41], which often suffer from damage-related breakdown at high intensities, preionized liquid plasmas allow access to new regimes of plasma optics and strong-field phenomena, such as high-order harmonic generation and tunneling ionization, driven by evanescent fields. Furthermore, the generation of intense and nonuniform evanescent fields under these extreme conditions opens up new opportunities to explore strong-field physics beyond the electric-dipole approximation [42]. Notably, under our experimental conditions, significant ponderomotive forces and magnetic fields are predicted to arise from the spatially varying evanescent field, as detailed in Appendixes A and B.

ACKNOWLEDGMENT

This work was partially supported by the MEXT Quantum Leap Flagship Program (MEXT Q-LEAP), Grant No. JPMXS0118068681.

DATA AVAILABILITY

The data that support the findings of this article are not publicly available upon publication because it is not technically feasible and/or the cost of preparing, depositing, and hosting the data would be prohibitive within the terms of this research project. The data are available from the authors upon reasonable request.

APPENDIX A: CALCULATED WAVE FORMS OF THE MIR LIGHT FIELD IN PREIONIZED AND PURE WATER OBTAINED BY SOLVING THE NONLINEAR PROPAGATION EQUATION

Figure 10 shows the evanescent and propagating fields of the MIR pulse as a function of the distance z inward from the surface of preionized and pure water, corresponding to with and without the NIR pump, respectively. The intensities of both the NIR pump and the MIR probe are $2 \times 10^{14}\,\mathrm{W/cm^2}$, corresponding to Fig. 5(d). Under these conditions, the ADK theory predicts that the electron density induced by the NIR pump exceeds the critical plasma density. Therefore, the MIR pulse becomes an evanescent field inside the ionized water. The results clearly show the exponential decay of the electric field within a scale of approximately 100 nm.

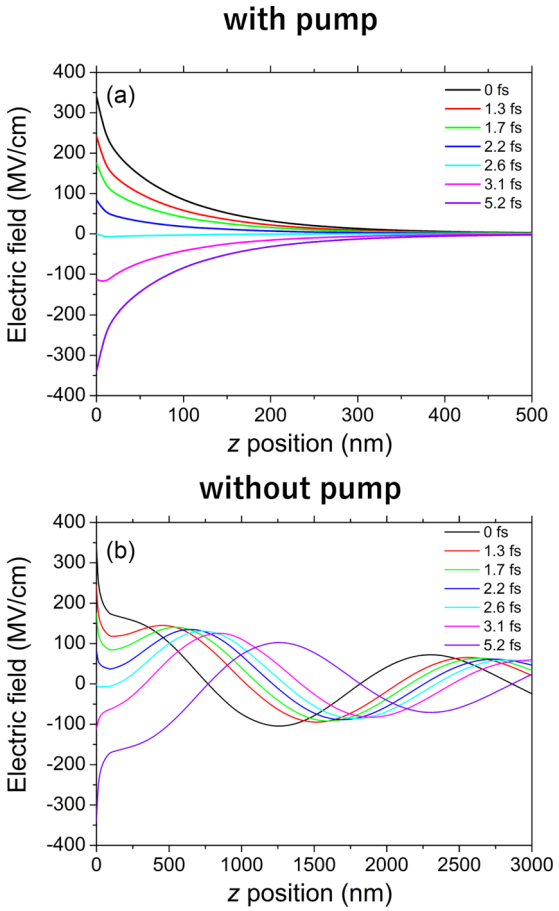


FIG. 10. Calculated wave forms of the MIR-drive pulse in preionized and pure water, corresponding to (a) with and (b) without NIR-pump pulses.

On the other hand, even without the pump, the MIR pulse itself can generate many electrons with a density that exceeds the critical plasma density, but only to a distance about 150 nm inward from the surface. Figure 10(b) also illustrates the decaying evanescent field inward from the surface. After the electron density drops below the critical plasma density, a propagating field reappears that exhibits oscillatory behavior. These spectra, calculated without the NIR pump, exhibit spectral broadening, corresponding to Fig. 4. This also leads to saturation of the harmonic yields due to the decrease in an interaction length.

APPENDIX B: POTENTIAL APPLICATIONS OF AN INTENSE NONUNIFORM EVANESCENT FIELD

Evanescent fields are widely used in various applications because of their nonuniform distributions [42,43]. Typically,

such a nonuniform field is generated by the near field of a plasmonic device [39,40,44]. Nonuniform near-field-induced HHG has been reported to exhibit dipole-forbidden emission due to the quadrupole contribution of the near field [39]. However, the usable electric field strength of such a device is limited by the damage by the optical field. In contrast, an evanescent field in a preionized liquid target has the potential to generate a more intense nonuniform field, which could enable studies of strong-field physics beyond the electric-dipole approximation [42].

Here, we highlight the characteristic features of an intense nonuniform evanescent field, which differ from those of a propagating light field. The evanescent electric field is approximately expressed as

$$E(z,t) = E_0 \exp(-\kappa k_0 z)\cos(\omega_0 t), \tag{B1}$$

where κ represents the imaginary part of the refractive index $n = i\kappa$. It characterizes a decay strength of an evanescent field. In this case the corresponding magnetic field is given by

$$B(z,t) = \kappa \frac{E_0}{c} \exp(-\kappa k_0 z)\sin(\omega_0 t). \tag{B2}$$

The phases of the evanescent electric and magnetic fields are out of phase by $\pi/2$, which distinguishes them from a propagating field, where the electric and magnetic fields are in phase. Equation (B2) shows that the magnetic field is amplified by κ, resulting in a stronger magnetic field in the case of a more rapid decay. In our experimental conditions, corresponding to Fig. 10(a), κ is about 10, which corresponds to an electron density generated by the NIR-pump pulse of $1 \times 10^{22}\,\mathrm{cm}^{-3}$. In this case, the corresponding magnetic field reaches 1.5 kT. Such a strong magnetic field can significantly influence the electron dynamics in ionized liquid plasmas.

In a nonuniform oscillating electromagnetic field, a charged particle experiences the ponderomotive force **F**, given by

$$\mathbf{F} = -\nabla U_p, \tag{B3}$$

where U_p represents the ponderomotive energy. The corresponding force to Fig. 10(a) is about $10^{-8}\,\mathrm{N}$, which is equivalent to the force that an electron experiences in an electric field of 660 MV/cm. In our case the ponderomotive energy strongly pushes the emitted electrons in the forward direction. The strong-field phenomena induced by the nonuniform field thus differ fundamentally from those induced by a propagating light field [45].

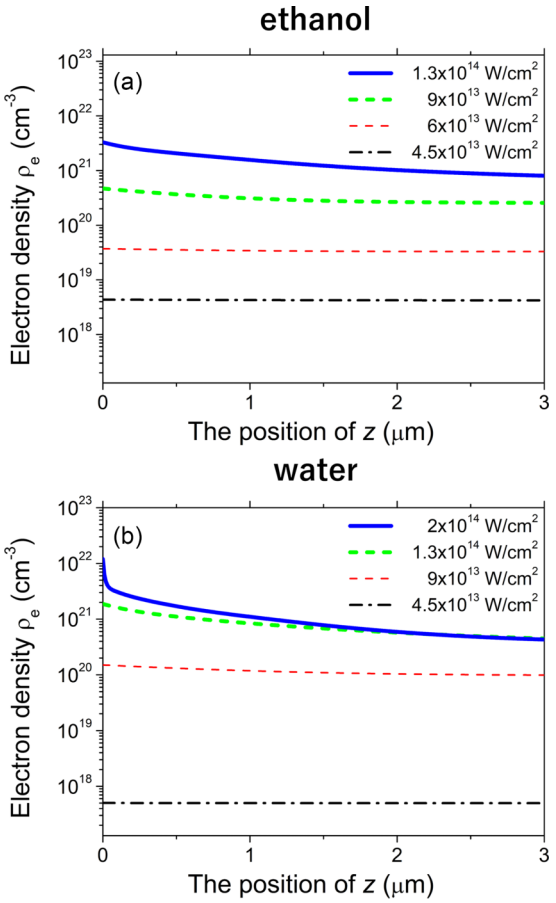


FIG. 11. Calculated electron densities ionized by the NIR pulses in (a) liquid ethanol and (b) water as a function of z.

APPENDIX C: ELECTRON DENSITIES INDUCED BY THE NIR-PUMP PULSES AS A FUNCTION OF z

Figure 11 shows the calculated electron densities induced by the NIR-pump pulses for various pump intensities as a function of z. For liquid ethanol, as shown in Fig. 11(a), at intensities of $9 \times 10^{13}\,\mathrm{W/cm^2}$ and $1.3 \times 10^{14}\,\mathrm{W/cm^2}$, the NIR-pump pulses can generate many electrons, with electron densities that exceed the critical plasma density for the MIR-drive pulse. For liquid water, this occurs at $1.3 \times 10^{13}\,\mathrm{W/cm^2}$ and $2 \times 10^{14}\,\mathrm{W/cm^2}$, as shown in Fig. 11(b). Furthermore, in water at an NIR-pump intensity of $2 \times 10^{14}\,\mathrm{W/cm^2}$, the calculated electron density rapidly decays near the surface. The electron density in this region also exceeds the critical plasma density for the NIR pump of 800 nm. Thus, the NIR-pump pulse decays due to the plasma-shutter effect, leading to a rapid decrease in electron density.

[1] P. B. Corkum and F. Krausz, Attosecond science, Nat. Phys. **3**, 381 (2007).

[2] G. Sansone, E. Benedetti, F. Calegari, C. Vozzi, L. Avaldi, R. Flammini, L. Poletto, P. Villoresi, C. Altucci, R. Velotta, S. Stagira, S. De Silvestri, and M. Nisoli, Isolated single-cycle attosecond pulses, Science **314**, 443 (2006).

[3] S. Ghimire, A. DiChiara, E. Sistrunk, P. Agostini, L. F. DiMauro, and D. A. Reis, Observation of high-order harmonic generation in a bulk crystal, Nat. Phys. **7**, 138 (2011).

[4] G. Vampa, T. J. Hammond, N. Thiré, B. E. Schmidt, F. Légaré, C. R. McDonald, T. Brabec, and P. B. Corkum, Linking high

harmonics from gases and solids, Nature (London) **522**, 462 (2015).

[5] K. Kaneshima, Y. Shinohara, K. Takeuchi, N. Ishii, K. Imasaka, T. Kaji, S. Ashihara, K. L. Ishikawa, and J. Itatani, Polarization-resolved study of high harmonics from bulk semiconductors, Phys. Rev. Lett. **120**, 243903 (2018).

[6] P. Xia, T. Tamaya, C. Kim, F. Lu, T. Kanai, N. Ishii, J. Itatani, H. Akiyama, and T. Kato, High-harmonic generation in GaAs beyond the perturbative regime, Phys. Rev. B **104**, L121202 (2021).

[7] G. Vampa, Y. S. You, H. Liu, S. Ghimire, and D. A. Reis, Observation of backward high-harmonic emission from solids, Opt. Express **26**, 12210 (2018).

[8] P. Xia, C. Kim, F. Lu, T. Kanai, H. Akiyama, J. Itatani, and N. Ishii, Nonlinear propagation effects in high harmonic generation in reflection and transmission from gallium arsenide, Opt. Express **26**, 29393 (2018).

[9] S. Yamada, T. Otobe, D. Freeman, A. Kheifets, and K. Yabana, Propagation effects in high-harmonic generation from dielectric thin films, Phys. Rev. B **107**, 035132 (2023).

[10] T. T. Luu, Z. Yin, A. Jain, T. Gaumnitz, Y. Pertot, J. Ma, and H. J. Wörner, Extreme-ultraviolet high-harmonic generation in liquids, Nat. Commun. **9**, 3723 (2018).

[11] A. Mondal, O. Neufeld, Z. Yin, Z. Noubakhsh, V. Svoboda, and H. J. Wörner, High-harmonic spectroscopy of low-energy electron-scattering dynamics in liquids, Nat. Phys. **19**, 1813 (2023).

[12] O. Alexander, J. C. T. Barnard, E. W. Larsen, T. Avni, S. Jarosch, C. Ferchaud, A. Gregory, S. Parker, G. Galinis, A. Tofful, D. Garratt, M. R. Matthews, and J. P. Marangos, Observation of recollision-based high-harmonic generation in liquid isopropanol and the role of electron scattering, Phys. Rev. Res. **5**, 043030 (2023).

[13] Y. H. Kim, H. Kim, S. C. Park, Y. Kwon, K. Yeom, W. Cho, T. Kwon, H. Yun, J. H. Sung, S. K. Lee, T. T. Luu, C. H. Nam, and K. T. Kim, High-harmonic generation from a flat liquid-sheet plasma mirror, Nat. Commun. **14**, 2328 (2023).

[14] A. Cavagna, M. Eder, E. Chowdhury, A. Kalouguine, J. Kaur, G. Mourou, S. Haessler, and R. Lopez-Martens, Continuous relativistic high-harmonic generation from a kHz liquid-sheet plasma mirror, Opt. Lett. **50**, 165 (2025).

[15] R. Zürl and H. Graener, High-harmonic generation of mid-IR pulses in simple liquids, Appl. Phys. B **66**, 213 (1998).

[16] A. D. DiChiara, E. Sistrunk, T. A. Miller, P. Agostini, and L. F. DiMauro, An investigation of harmonic generation in liquid media with a mid-infrared laser, Opt. Express **17**, 20959 (2009).

[17] J. Xu, D. Chen, and S. Meng, Probing laser-induced plasma generation in liquid water, J. Am. Chem. Soc. **143**, 10382 (2021).

[18] W. Liu, S. Petit, A. Becker, N. Aközbek, C. Bowden, and S. Chin, Intensity clamping of a femtosecond laser pulse in condensed matter, Opt. Commun. **202**, 189 (2002).

[19] E. Ponomareva, A. Ismagilov, S. Putilin, and A. N. Tcypkin, Plasma reflectivity behavior under strong subpicosecond excitation of liquids, APL Photonics **6**, 126101 (2021).

[20] J. Li, Z. Nie, Y. Y. Zheng, S. Dong, and Z.-H. Loh, Elementary electron and ion dynamics in ionized liquid water, J. Phys. Chem. Lett. **4**, 3698 (2013).

[21] T. Toigawa, M. Gohdo, K. Norizawa, T. Kondoh, K. Kan, J. Yang, and Y. Yoshida, Examination of the formation process of pre-solvated and solvated electron in n-alcohol using femtosecond pulse radiolysis, Radiat. Phys. Chem. **123**, 73 (2016).

[22] G. McCaul, M. Runge, M. Woerner, D. Talbayev, T. Elsaesser, and D. I. Bondar, Tuning the terahertz response of liquids by creating polar many-body excitations, Phys. Rev. A **112**, L011101 (2025).

[23] F. Lu, P. Xia, Y. Matsumoto, T. Kanai, N. Ishii, and J. Itatani, Generation of sub-two-cycle CEP-stable optical pulses at 3.5 μm from a KTA-based optical parametric amplifier with multiple-plate compression, Opt. Lett. **43**, 2720 (2018).

[24] T. Yang, T. Kurihara, Y. Hua, T. Mizuno, T. Kanai, S. Ashihara, Y. Harada, and J. Itatani, Enhancement of high harmonic generation in liquid water by resonant excitation in the mid-infrared, Appl. Phys. Express **17**, 122006 (2024).

[25] A. Watanabe, H. Saito, Y. Ishida, M. Nakamoto, and T. Yajima, A new nozzle producing ultrathin liquid sheets for femtosecond pulse dye lasers, Opt. Commun. **71**, 301 (1989).

[26] E. Sani and A. Dell'Oro, Spectral optical constants of ethanol and isopropanol from ultraviolet to far infrared, Opt. Mater. (NY) **60**, 137 (2016).

[27] J.-J. Max and C. Chapados, Isotope effects in liquid water by infrared spectroscopy, III. H_2O and D_2O spectra from 6000 to 0 cm^{-1}, J. Chem. Phys. **131**, 184505 (2009).

[28] L. Sudrie, A. Couairon, M. Franco, B. Lamouroux, B. Prade, S. Tzortzakis, and A. Mysyrowicz, Femtosecond laser-induced damage and filamentary propagation in fused silica, Phys. Rev. Lett. **89**, 186601 (2002).

[29] A. Couairon and A. Mysyrowicz, Femtosecond filamentation in transparent media, Phys. Rep. **441**, 47 (2007).

[30] NIST, NIST Chemistry Webbook, https://webbook.nist.gov/chemistry/.

[31] R. W. Boyd, *Nonlinear Optics,* 3rd ed. (Academic Press, New York, 2008).

[32] H. Zhang, Y. Zhang, S. Lin, Y. Zhang, A. Chen, Y. Jiang, S. Li, and M. Jin, Influence of pressure on spectral broadening of femtosecond laser pulses in air, Phys. Plasma **28**, 043302 (2021).

[33] S. Hilal, M. Melnik, A. Ismagilov, A. Tsypkin, and S. Kozlov, Determination of plasma properties in liquid jets through time-resolved experiments on third harmonic reflection dynamics, Opt. Lett. **49**, 2990 (2024).

[34] M. V. Ammosov, N. B. Delone, and V. P. Krainov, Tunnel ionization of complex atoms and of atomic ions in an alternating electromagnetic field, Sov. Phys. JETP **64**, 1191 (1986).

[35] A. Ghalgaoui, L.-M. Koll, B. Schütte, B. P. Fingerhut, K. Reimann, M. Woerner, and T. Elsaesser, Field-Induced tunneling ionization and terahertz-driven electron dynamics in liquid water, J. Phys. Chem. Lett. **11**, 7717 (2020).

[36] M. Woerner, B. P. Fingerhut, and T. Elsaesser, Field-induced electron generation in water: Solvation dynamics and many-body interactions, J. Phys. Chem. B **126**, 2621 (2022).

[37] L. V. Keldysh, Ionization in the field of a strong electromagnetic wave, Sov. Phys. JETP **20**, 1307 (1965).

[38] J. Xu and S. Meng, High-harmonic generation and femtosecond-resolved ultrafast dynamics in liquid water, J. Phys. Chem. Lett. **16**, 5295 (2025).

[39] S. A. Jalil, K. M. Awan, J. Baxter, G. Bart, D. N. Purschke, T. Fennel, D. M. Villeneuve, A. Staudte, P. Berini, T. Brabec,

L. Ramunno, and G. Vampa, Spectroscopic signatures of plasmonic near-fields on high-harmonic emission, Laser Photonics Rev. **17**, 2300448 (2023).

[40] A. M. Kern and O. J. F. Martin, Strong enhancement of forbidden atomic transitions using plasmonic nanostructures, Phys. Rev. A **85**, 022501 (2012).

[41] T. Mizuno, K. Takeuchi, K. Kaneshima, N. Ishii, T. Kanai, and J. Itatani, Resonant-like field enhancement by nanoscale grating-coupled propagating surface plasmons and localized surface plasmons in the mid-infrared range: Implications for ultrafast plasmonic electron sources, ACS Appl. Nano Mater. **2**, 7067 (2019).

[42] M. F. Ciappina, J. Biegert, R. Quidant, and M. Lewenstein, High-order-harmonic generation from inhomogeneous fields, Phys. Rev. A **85**, 033828 (2012).

[43] A. Husakou, S.-J. Im, and J. Herrmann, Theory of plasmon-enhanced high-order harmonic generation in the vicinity of metal nanostructures in noble gases, Phys. Rev. A **83**, 043839 (2011).

[44] T. Iwasa and K. Nobusada, Nonuniform light-matter interaction theory for near-field-induced electron dynamics, Phys. Rev. A **80**, 043409 (2009).

[45] M. Mochol and Sacha, Artificial magnetic field induced by an evanescent wave, Sci. Rep. **5**, 7672 (2015).